Water Research 200 (2021) 117300

Contents lists available at ScienceDirect

Water Research

journal homepage: www.elsevier.com/locate/watres

Carbon and methane cycling in arsenic-contaminated aquifers

Emiliano Stopelli[a,#,*], Vu T. Duyen[b], Henning Prommer[c,d], Martyna Glodowska[e], Andreas Kappler[e], Magnus Schneider[f], Elisabeth Eiche[f], Alexandra K. Lightfoot[a], Carsten J. Schubert[h,i], Pham K.T. Trang[b], Pham H. Viet[b], Rolf Kipfer[a,i], Lenny H.E. Winkel[a,i], Michael Berg[a,j,*], AdvectAs team members[g]

[a] Eawag, Swiss Federal Institute of Aquatic Science and Technology, Department Water Resources and Drinking Water, 8600 Dübendorf, Switzerland
[b] Key Laboratory of Analytical Technology for Environmental Quality and Food Safety (KLATEFOS), VNU University of Science, Vietnam National University, Hanoi, Vietnam
[c] CSIRO Land and Water, 6014 Floreat, WA, Australia
[d] School of Earth Sciences, University of Western Australia, Crawley, WA 6009, Australia
[e] Geomicrobiology, Center for Applied Geosciences, University of Tübingen, 72076 Tübingen, Germany
[f] Institute of Applied Geosciences, Karlsruhe Institute of Technology, 76131 Karlsruhe, Germany
[g] AdvectAs team members—listed in the SI
[h] Eawag, Swiss Federal Institute of Aquatic Science and Technology, Department Surface Waters Research & Management, 6047 Kastanienbaum, Switzerland
[i] Institute of Biogeochemistry and Pollutant Dynamics, ETH Zurich, 8092 Zurich, Switzerland
[j] UNESCO Chair on Groundwater Arsenic within the 2030 Agenda for Sustainable Development, School of Civil Engineering and Surveying, University of Southern Queensland, QLD 4350, Australia

ARTICLE INFO

Article history:
Received 19 February 2021
Revised 22 May 2021
Accepted 24 May 2021
Available online 27 May 2021

Keywords:
Groundwater quality
Drinking water
Geogenic As contamination
Heterogeneity
Organic matter
Carbon isotope $\delta^{13}C$

ABSTRACT

Geogenic arsenic (As) contamination of groundwater is a health threat to millions of people worldwide, particularly in alluvial regions of South and Southeast Asia. Mitigation measures are often hindered by high heterogeneities in As concentrations, the cause(s) of which are elusive. Here we used a comprehensive suite of stable isotope analyses and hydrogeochemical parameters to shed light on the mechanisms in a typical high-As Holocene aquifer near Hanoi where groundwater is advected to a low-As Pleistocene aquifer. Carbon isotope signatures ($\delta^{13}C$-CH_4, $\delta^{13}C$-DOC, $\delta^{13}C$-DIC) provided evidence that fermentation, methanogenesis and methanotrophy are actively contributing to the As heterogeneity. Methanogenesis occurred concurrently where As levels are high (>200 µg/L) and DOC-enriched aquitard pore water infiltrates into the aquifer. Along the flowpath to the Holocene/Pleistocene aquifer transition, methane oxidation causes a strong shift in $\delta^{13}C$-CH_4 from -87‰ to +47‰, indicating high reactivity. These findings demonstrate a previously overlooked role of methane cycling and DOC infiltration in high-As aquifers.

1. Introduction

The health of tens of millions of people worldwide is affected by chronic exposure to arsenic-polluted groundwater resources (WHO, 2011; Karagas et al., 2015; Podgorski and Berg, 2020). Diseases caused by this exposure are particularly common in the floodplains and deltas of the large East and South Asian river systems (Smith et al., 2000; Harvey et al., 2002; McArthur et al., 2004; Berg et al., 2007; Fendorf et al., 2010; Zhang et al., 2017). There, the natural abundance of bioavailable natural organic matter (OM) in geologically young Holocene depositions often leads to hydrogeochemical conditions under which the reductive dissolution of As-bearing Fe(III) (oxyhydr)oxide minerals triggers As release and widespread groundwater As pollution (Smedley and Kinniburgh, 2002; Islam et al., 2004; Stuckey et al., 2016). In contrast, older sediments of the Pleistocene period generally exhibit less reducing aquifer conditions, with As concentrations usually <10 µg/L.

A striking feature of As-affected aquifers is the high, local-scale spatial variability of As concentrations (van Geen et al., 2006; Eiche et al., 2008; Fendorf et al., 2010; Cozzarelli et al., 2016; Ziegler et al., 2017; Polya et al., 2019), which is thought to be linked to hydrogeological heterogeneities and to associated variations in dominating redox processes. Besides Fe(III) (oxyhydr)oxides and other redox-sensitive mineral phases, the abun-

* Corresponding authors.
E-mail addresses: emiliano.stopelli@eawag.ch (E. Stopelli), michael.berg@eawag.ch (M. Berg).
Present address: Nagra, National Cooperative for the Disposal of Radioactive Waste, International Services and Projects, 5430 Wettingen, Switzerland

https://doi.org/10.1016/j.watres.2021.117300

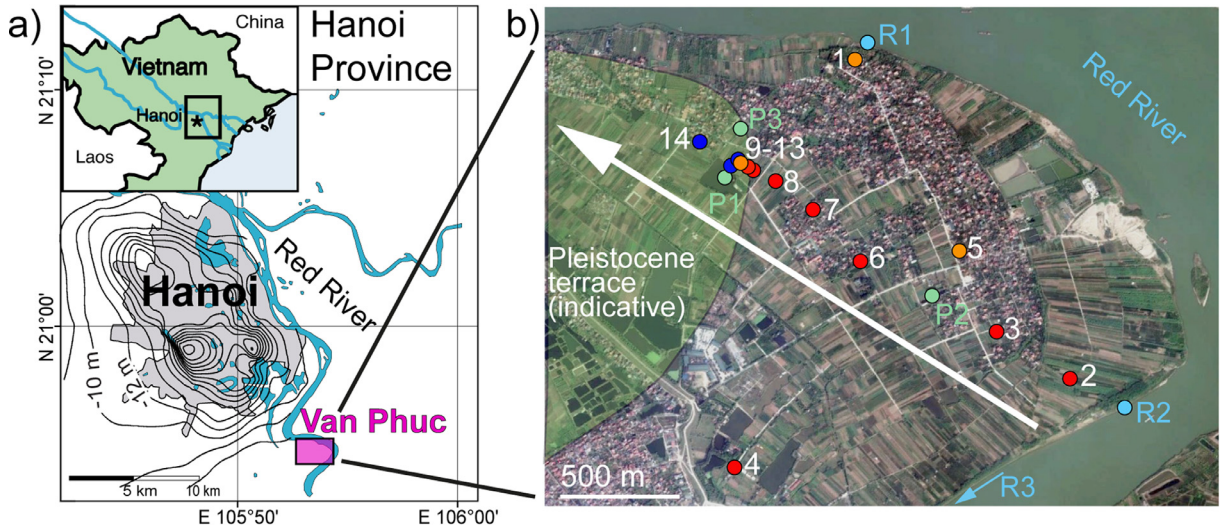

Fig. 1. Field site and sampling locations. **A**) Regional setting of the Van Phuc field site in the vicinity of Hanoi. Groundwater withdrawal in Hanoi causes large cones of depression in the Pleistocene aquifer (black contour lines), inducing a fairly steady groundwater advection in the aquifers beneath Van Phuc (Berg et al., 2008; van Geen et al., 2013). **B**) Satellite image of the study site (Google Earth). The white arrow indicates the general groundwater flow direction towards Hanoi (van Geen et al., 2013). The coloured dots depict the locations of the studied groundwater wells (numbers in white, red dots for As >100 µg/L, orange dots for As 10–100 µg/L, blue dots for As <10 µg/L, well depths ranging from 18 to 53 m b.g.l.). Sampling locations for river and riverbank water (light blue), and for pond water (light green) are also shown. Figure adapted from Stopelli et al. Stopelli et al. (2020).

dance of dissolved sulphate (SO_4^{2-}) and the formation of As-sulphide minerals has also been recognised to impact the mobility of As (Bostick and Fendorf, 2003; Buschmann and Berg, 2009). Furthermore, the bioavailable OM in young riverbank deposits, ponds or channel infill plays an important role in creating hot spots of As mobilisation, while older sedimentary OM, which tends to be more recalcitrant, is of lower significance (Harvey et al., 2002; McArthur et al., 2004; Rowland et al., 2007; Polizzotto et al., 2008; Neumann et al., 2010; Postma et al., 2012; Lawson et al., 2016; Kulkarni et al., 2017; Richards et al., 2019; Glodowska et al., 2020a; Wallis et al., 2020). However, in that context the role of methane (CH_4) cycling has rarely been considered, especially in natural settings (Polya et al., 2019), although several studies detected CH_4 in As-contaminated aquifers (Liu et al., 2009; Postma et al., 2012, 2016; Sø et al., 2018) and indicated that elevated CH_4 and As concentrations might be related (Buschmann and Berg, 2009; Sracek et al., 2018).

On larger scales (100 m to kilometre) and based on the genesis and the resulting mineralogical characteristics of Pleistocene and Holocene sediments, high and low As aquifers often show highly contrasting redox conditions. They are found adjacent to each other, separated by redox transition zones (RTZ). Generally, the formation and stability of RTZ is linked to a variety of factors, including the interaction of transport processes, microbial activity and the stability of As host mineral phases, mainly Fe-bearing phases.

Here, we present a first detailed isotope study of CH_4 and C cycling and its potential impact on As mobility at the metre to kilometre scale. Our field site at Van Phuc near Hanoi (Vietnam) has previously been the subject of a wide range of comprehensive studies that investigated geological, hydrochemical, microbial, lithological and anthropogenic characteristics that are common at many As-polluted aquifers in Asia (Berg et al., 2008; Eiche et al., 2008; van Geen et al., 2013; Stahl et al., 2016; Eiche et al., 2017; Nghiem et al., 2020; Stopelli et al., 2020). The Van Phuc site features a relatively stable lateral groundwater flow induced by large-scale groundwater pumping in nearby Hanoi (Berg et al., 2008; van Geen et al., 2013) (Fig. 1A). Surface water from the Red River infiltrates through OM-rich riverbed sediments, where As is mobilised by reductive dissolution, before migrating through a Fe-reducing high-As Holocene aquifer and across a redox transition zone (RTZ) into an older, low-As aquifer of Pleistocene deposits (Fig. 1B).

Both aquifers are capped by a silty aquitard of 15–22 m thickness that contains sandy lenses and intercalations of OM (Berg et al., 2008; Eiche et al., 2008). The study site also hosts several eutrophic ponds that are used for aquaculture.

We use a comprehensive suite of isotopic analyses (δ^{13}C-DOC, δ^{13}C-CH_4, δ^{13}C-DIC, plus stable water isotopes δ^{18}O and δ^{2}H) to identify OM sources, as well as to elucidate processes of carbon cycling and the potential role of CH_4 cycling on As mobilisation.

2. Materials and methods

2.1. Experimental design

Groundwater samples were collected in July 2018 and again in April 2019 in the village of Van Phuc, which is located along a Red River meander some 15 km southeast of Hanoi, Vietnam. Nine new monitoring wells were installed between the riverbank and the redox transition zone (RTZ) in December 2018, where previous hydrochemical data were scarce, and an additional well was recovered. Overall, a total of 29 groundwater samples (well depths 18 to 53 m b.g.l., 1-metre well screen) and nine surface water samples (Red River, riverbank pore water, ponds) were collected for analyses.

2.2. Sample collection

Groundwater samples were collected with an electric submersion pump after the stabilisation of pH, redox potential E_h, oxygen and conductivity; these were measured using a daily calibrated portable multi-analyser (WTW 3630). The E_h values were normalised to the standard hydrogen electrode (SHE). River and pond water samples were collected in a bucket. Riverbank pore water was sampled by pushing a hollow stainless-steel rod (1 cm I.D.) some 25–30 cm into the sediment. The hollow rod was screened at the tip and pore water was drawn with a syringe through a tube from the inner part of the rod (Stahl et al., 2016; Stopelli et al., 2020). The field parameters (O_2, pH, E_h, conductivity, temperature)

of the samples were immediately measured. Alkalinity was determined directly in the field by titration as HCO_3^- alkalinity (Merck Mcolortest 11,109 test kit) and expressed as mg C/L. Because alkalinity may not solely depend on dissolved HCO_3^-, dissolved inorganic carbon DIC concentrations were calculated with PHREEQC (v3.4.0) (Parkhurst and Appelo, 2013) based on the measured hydrochemical parameters. All values lower than the Limits of Quantification (LOQ) of each method were set as half of the LOQ for visualisation in the graphs. Sample aliquots for hydrochemical analyses were all filtered through 0.45-µm cellulose acetate into pre-rinsed polypropylene bottles; three aliquots also underwent acidification to pH<2 to improve their stability (one for metals and trace elements, NH_4^+ and PO_4^{3-} acidified with 1% v/v HNO_3, one for As(III) acidified with 1% v/v HNO_3 after passing the sample through an As(III)/As(V) separation cartridge (MetalSoft), and one for DOC acidified with 1% v/v HCl). Immediately after collection, all aliquots were stored at 4 °C and protected from light until the analyses. Detailed descriptions of the sampling technique and quality control for the hydrochemical parameters are available in Stopelli et al. Stopelli et al. (2020).

2.3. Hydrochemical analyses

Major cations and trace elements were determined by Inductively Coupled Plasma Mass Spectrometry (ICP-MS, Agilent 7500 and 8900), dissolved nitrogen (DN) and dissolved organic carbon (DOC, which does not include dissolved methane) with a total N and C analyser (Shimadzu TOC-L CSH), NH_4^+ and ortho-PO_4^{3-} with photometry using the indophenol and molybdate methods, respectively, and anions by ion chromatography (Metrohm 761 Compact IC).

2.4. Stable isotope analyses

The water δ^2H and $\delta^{18}O$ ratios were determined from 8-mL samples collected in amber glass vials without headspace and were analysed using a cavity ringdown spectrometer (Picarro). The replicate standard and sample measurements indicated reproducibility within 0.5‰ for $\delta^{18}O$ and 3‰ for δ^2H. The δ^2H and $\delta^{18}O$ ratios were normalised to Vienna Standard Mean Ocean Water (VSMOW).

The samples for total methane determination were collected directly from the pumping tube by inserting a needle into 5-mL evacuated glass vials (Labco819W). A headspace of half to two-thirds of the total volume was left, and the vials were immediately frozen on dry ice in an upside-down position to trap the gas phase above the frozen water in the vial headspace and to ensure sample stabilisation. Methane concentrations were analysed after complete sample thawing by gas chromatography (Shimadzu GC-2014) via the headspace equilibration method following the procedure reported in Sø et al. Sø et al. (2018). Samples for $\delta^{13}C$-CH_4 were collected in April 2019 in 120-mL serum bottles, filled anoxically by water overflow, poisoned with 20 mg Cu(I)Cl, sealed with butyl–rubber thick stoppers and aluminium crimps and preserved at +4 °C until analysis. In the laboratory, a 20 mL nitrogen (N_2) headspace was inserted for overnight equilibration. First, the samples were injected and concentrated with a series of traps in a trace gas unit (T/GAS PRECON, Micromass UK Ltd). The purified gas was then analysed with an isotope ratio mass spectrometer (IRMS; GV Instruments, Isoprime). The replicate sample and standard measurements were reproducible within 2‰. The $\delta^{13}C$-CH_4 data are normalised to the Vienna Pee Dee Belemnite (VPDB) reference standard.

Samples for $\delta^{13}C$-DIC were collected in July 2018, filtered through pre-combusted 0.7-μm glass fibre mesh into 40-mL glass amber vials with black butyl septa, and stored at +4 °C until analysed. Samples for $\delta^{13}C$-DOC were filtered through 0.7-µm glass fibres mesh into 40-mL glass amber vials with white silicon-Teflon septa and acidified to pH<2 with HCl, analytical grade. Samples for $\delta^{13}C$-DOC were collected in July 2018 and in April 2019 for the newly installed wells. Groundwater from six wells was collected both times to check for the comparability of isotopic values between the different sampling campaigns (double values in Table S1). Isotopic ratios were determined with an elemental analyser coupled to an isotope ratio mass spectrometer (EA-IRMS, EA Thermo Flash 2000 and IRMS Thermo Delta V) at the Stable Isotope Ecology Laboratory, University of Georgia. Replicate sample measurements resulted in an analytical reproducibility of 0.5‰, while repeated sampling of the same well in two different field campaigns yielded a slightly higher variability of up to 1‰ for DOC and 2‰ for DIC. The $\delta^{13}C$-DIC and $\delta^{13}C$-DOC values are normalised to the Vienna Pee Dee Belemnite (VPDB) reference standard.

Samples for $\delta^{15}N$-NH_4^+ were collected in July 2018, filtered through a 0.45-µm cellulose acetate filter into 250- and 500- mL propylene bottles and immediately frozen at −20 °C until analysed. In the laboratory, N was concentrated on filters following the ammonia diffusion method as described in Holmes et al. (Holmes et al., 1998), and the filters were further analysed via EA-IRMS at the Stable Isotope Ecology Laboratory, University of Georgia. The replicate standard measurements indicated an analytical reproducibility within 1‰. The $\delta^{15}N$-NH_4^+ values are normalised to air reference.

2.5. Statistical analyses

Statistical tests and probability calculations were carried out using the PAST software, version 3.17 (Hammer et al., 2001).

3. Results and discussion

3.1. Hydrology and hydrogeochemical evolution of As contamination

A comprehensive set of stable isotope signatures and hydrochemical parameters (see Methods) was determined from groundwater and surface water samples collected along a 2-km long transect that follows the average groundwater flow direction towards Hanoi, as inferred from previous hydrological, hydrochemical and numerical studies (Fig. 1) (van Geen et al., 2013; Stopelli et al., 2020; Wallis et al., 2020). River water infiltration is the main source of groundwater recharge at the study site with young, OM- and Fe(III)-rich riverbank sediments (Fig. 2) creating a hot spot of arsenic release at the Red River – groundwater interface (Stahl et al., 2016; Stopelli et al., 2020; Wallis et al., 2020). Dissolved As is then advected into and within the Holocene aquifer where concentrations initially range between 20 and 200 µg/L (Fig. 2, wells 2 to 5), hereafter indicated as flowpath 1.

Further along the groundwater flow direction, dissolved As reaches up to 540 µg/L in the Holocene aquifer (Fig. 2, wells 6 to 8). The highest dissolved As concentrations are found in the wells that also show the largest concentrations of dissolved organic carbon (DOC), ammonium (NH_4^+) and dissolved methane (CH_4), that is 5–7 mg DOC/L, 50–65 mg NH_4-N/L and 40–58 mg CH_4/L, respectively (Fig. 2 and Fig. S6 for NH_4^+). The water isotope signatures in these wells ($\delta^{18}O$ −6 ± 1‰) are indicative of evaporative water that locally infiltrates from the aquitard into the aquifer (Fig. 2), rather than of water originating from Red River bank infiltration. Sediment coring revealed substantial lithological heterogeneity in the clayey aquitard deposits including sandy intercalations, caused by alternating riverine and marine depositions during the Holocene period (Eiche et al., 2008, 2017; Trung et al., 2020; Kontny et al., 2021). It was also shown that aquitard depositions contain up to 9 wt.% of sedimentary OM (Eiche et al., 2008; Glodowska et al., 2020a). The DOC-enriched pore water (5–7 mg C/L, see Fig. 2) that

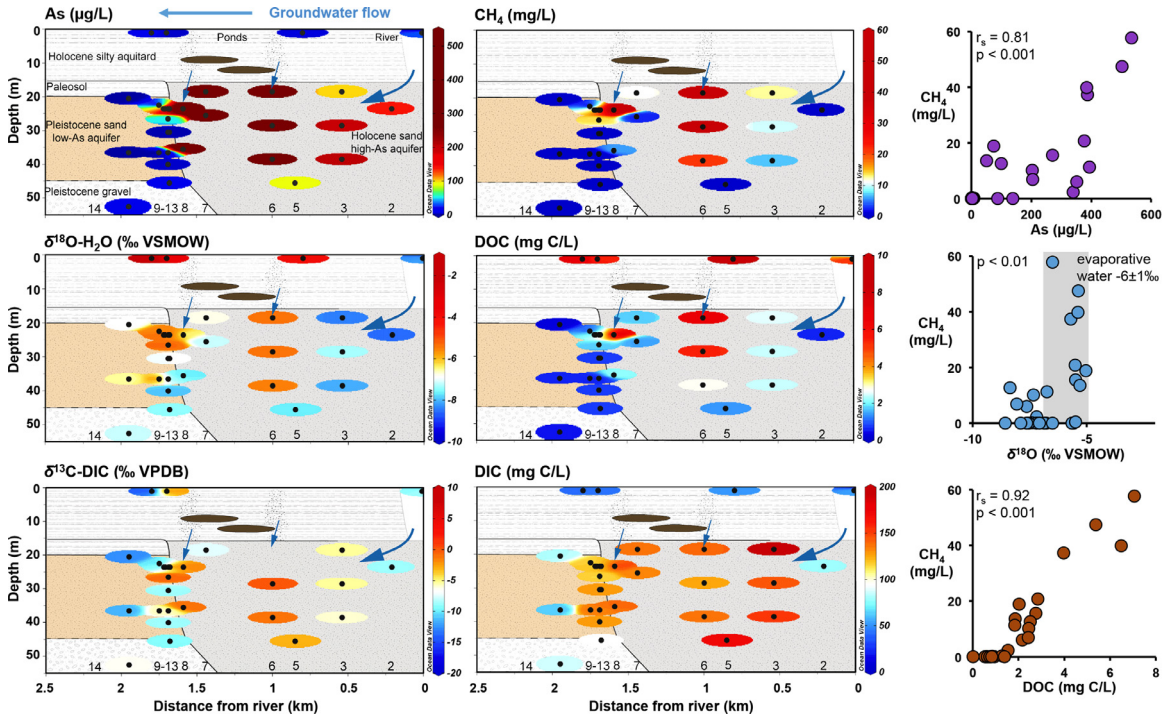

Fig. 2. Vertical cross-sections of groundwater parameters along the 2-km transect. Left and centre panels: Concentrations of As, CH_4, DOC and DIC, as well as isotope signatures of δ^{13}C-DIC and δ^{18}O of groundwater, surface water and riverbank samples (n_{tot}=38) collected along the studied transect depicted in Fig. 1. The black dots indicate the longitudinal positions and depths of the well screens with consecutive well numbers indicated above the x-axes. Sediment types are labelled in the As panel (top left), and shaded in different colours for the aquifers, with grey colour marking the Fe-reducing Holocene aquifer and beige colour marking the markedly less reducing Pleistocene aquifer. The colouring of the hydrochemical parameters is scaled to the maximum value in each panel (plotted with Ocean Data View, https://odv.awi.de). Blue arrows indicate the dominant horizontal groundwater flow from the riverbank through the Holocene aquifer (flowpath 1) and the localised (comparatively slow) vertical infiltration of pore water aquitard/aquifer hydraulic connections (flowpath 2). The boundaries separating the aquifers and the aquitard are schematically indicated. Right panels: Bivariate plots of CH_4/As, CH_4/δ^{18}O, and CH_4/DOC for the wells along the transect (n = 27), with the significance of Spearman's correlation coefficient r_s indicated.

evolves as it percolates through the sandy intercalations, creates locally highly reducing conditions as it egresses into the underlying aquifer, hereafter indicated as flowpath 2. Our mixing calculations based on the water isotope ratios (δ^{18}O and δ^{2}H) suggest that groundwater collected just below the aquitard (i.e., wells 6a and 8a in Fig. 2) consist of up to 92% aquitard pore water (see supplementary section SI.1 for calculations along with aquitard pore water compositions).

At the RTZ that marks the interface between the Holocene and the Pleistocene aquifers, both dissolved As and Fe concentrations sharply decrease (Fig. 2, wells 9 to 13, and Fig. S2) while Mn concentrations increase (Fig. S2). High-resolution mineralogical analyses of a sediment core that was drilled through the RTZ, demonstrate the presence of newly formed As-bearing mixed-valent Fe oxides (Kontny et al., 2021). This finding suggests that Fe^{2+} is advected from the Holocene aquifer into the RTZ, where it induces the transformation of Fe(III)(oxyhydr)oxides into a sequence of Fe(II) or mixed-valence Fe(II/III) phases (siderite, pyrite, goethite and haematite coatings, and magnetite; Kontny et al., 2021), accompanied by net As sorption and incorporation. Further along the groundwater flowpaths into the Pleistocene aquifer, As sorption onto the abundant Fe(oxyhydr)oxides of the Pleistocene sands attenuates the As concentrations to below 5 µg/L (Eiche et al., 2008; Rathi et al., 2017; Neidhardt et al., 2018) (Fig. 2, wells 14).

3.2. Sources of dissolved organic matter

The isotopic signatures of dissolved organic carbon (δ^{13}C-DOC, Fig. 3A) point to two distinct sources of OM, namely to (i) OM originating from riverbank sediments (δ^{13}C-DOC −28.0 ± 1‰ to −27.5 ± 1‰), and (ii) sedimentary OM embedded in the aquitard (δ^{13}C-TOC between −27±1‰ and −23±1‰) (Eiche et al., 2017). These signatures are indicative of OM derived from higher plant material and freshwater algae (Fry and Sherr, 1984; Campeau et al., 2017; Eiche et al., 2017). Additional DOC is possibly sourced from within the aquifer itself where isolated intercalations of up to 1 wt.% of OM exist with δ^{13}C-TOC signatures around −25‰ (Eiche et al., 2017). However, the aquifer's average TOC content is very low (<0.03 wt.% (Eiche et al., 2008)) and therefore unlikely to provide a sizeable contribution to driving biogeochemical transformations. This is in agreement with a recent reactive transport modelling analysis of the Van Phuc site that suggested negligible OM reactivity in the Holocene aquifer sands, while identifying the riverbank-groundwater interface as the dominant hotspot for OM turnover and associated As release (Wallis et al., 2020).

Overall, taking into account that (i) the highest DOC (5–7 mg/L) concentrations are present below the aquitard/Holocene aquifer hydraulic connections and (ii) the water isotopes indicate pore water infiltration from the aquitard, we conclude that the elevated DOC concentrations and the corresponding δ^{13}C-DOC signatures in parts of the Holocene aquifer (Fig. 2 and Fig. 3A, wells 4, 6a, 8a) are indicative of OM infiltrating from the aquitard.

3.3. Fermentation of dissolved organic carbon

Compared to the aquitard sedimentary δ^{13}C-TOC signatures of −20‰ to −27‰ at the site (Eiche et al., 2008) (flowpath 2) and to the δ^{13}C-DOC signatures of −27.5 ± 1‰ to −28±1‰ in riverbank porewater (flowpath 1), the δ^{13}C-DOC values in the studied groundwaters (−28±1‰ to −31±1‰) were slightly lower (Fig. 3A). This observation is consistent with the occurrence of anaerobic fermentation of OM to small molecules including, e.g., propionate

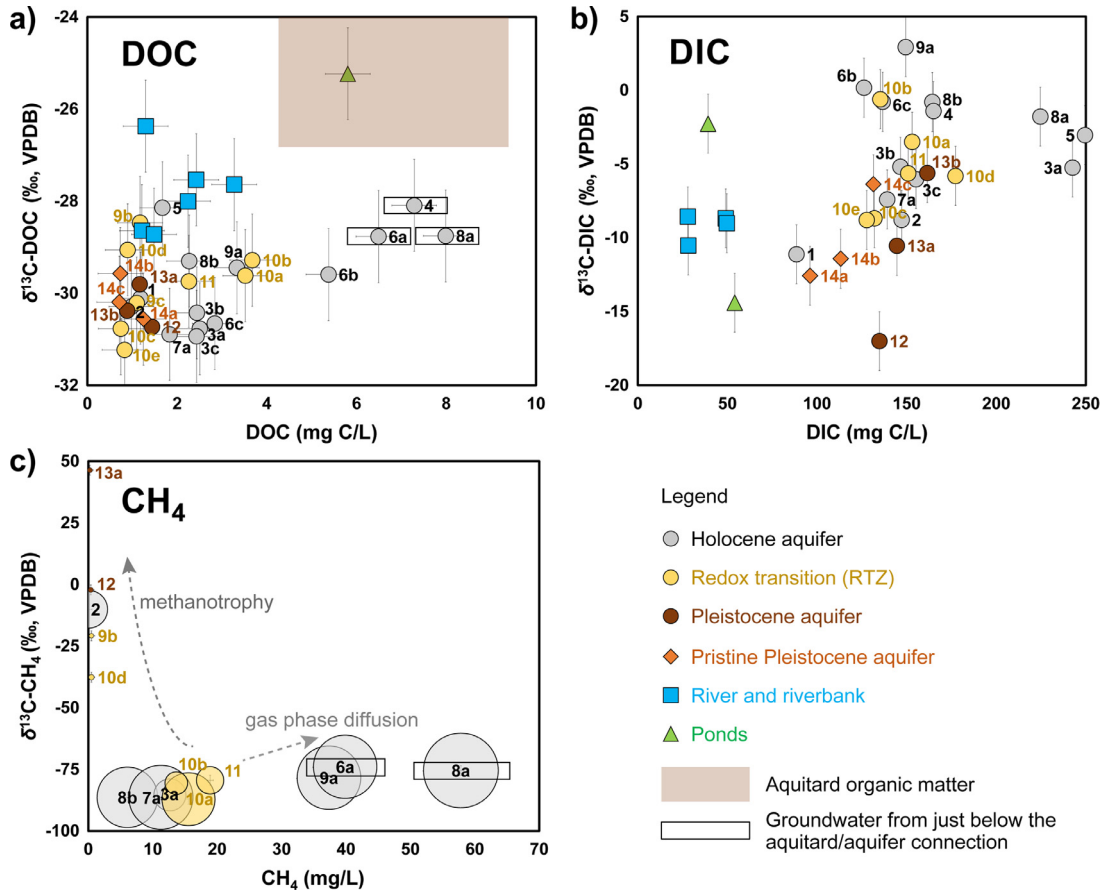

Fig. 3. Plots of carbon species and isotope signatures in the Holocene aquifer, at the redox transition and in the Pleistocene aquifer. **A**) δ^{13}C-DOC and DOC conc.; **B**) δ^{13}C-DIC and DIC conc.; **C**) δ^{13}C-CH_4 and CH_4 conc., where the dot size is proportional to the corresponding As concentration. The data points are numbered by the progressive distance from the river and a letter for increasing depth in cases of nested multilevel wells (see Table S1 for original data). The flat rectangles indicate groundwater from just below the aquitard/aquifer connection. The brown shading in panel a) represents δ^{13}C-TOC values of OM in aquitard sediment cores drilled between the monitoring wells 6 and 8 (Eiche et al., 2017), and of DOC concentrations in aquitard pore water extracted from cores at 16–18 m depth at well 6 (Supplementary material section SI.1). Whiskers represent standard deviation for each parameter, resulting from analytical uncertainty.

and acetate, a process that is characterised by a generally very small isotopic enrichment or even some depletion (Botsch and Conrad, 2011; Conrad et al., 2014). Moreover, our recent microbiological companion study (Glodowska et al., 2021) identified active and abundant bacterial communities capable of fermentative metabolism in all groundwater samples. Fermentative metabolisms generally produce CO_2, H_2 and a broad range of short chain C compounds from larger organic molecules and hence transform rather recalcitrant OM to more bioavailable compounds (McMahon and Chapelle, 1991; Chapelle, 2000). Subsequently, fermentation products may serve as substrates for both methanogenesis and the microbial reduction of Fe(III) (oxyhydr)oxides (Glodowska et al., 2020a).

3.4. DIC-isotopes indicative of methanogenesis and methanotrophy

Dissolved inorganic carbon (DIC) concentrations successively rise along the groundwater flowpath 1 from 18 mg C/L in the Red River to 23–28 mg C/L in riverbank pore water, and generally reach 100–200 mg C/L in the Holocene aquifer after a few hundred meters (Fig. 2 and 3B). This increase in DIC is attributed to both the dissolution of carbonate minerals and the high biogeochemical turnover of the freshly deposited OM in the riverbank sediments (Stahl et al., 2016; Wallis et al., 2020), likely followed by much more slowly progressing fermentation reactions within the Holocene aquifer (Stopelli et al., 2020; Glodowska et al., 2021).

Our carbon isotope δ^{13}C-DIC data reveal a more complex picture compared to the DIC concentrations alone (Fig. 2 and Fig. 3B). The almost uniform isotopic DIC signatures of −8.6 ± 2‰ to −11.1 ± 2‰ in river water, riverbank pore water and in Holocene groundwater close to the river (Fig. 3B, wells 1 and 2) reflect atmospheric CO_2 (−8‰ to −9‰) and dissolution of freshwater carbonates (CO_3^{2-}, +5‰ to −15‰), while the influence of OM oxidation (−10‰ to −25‰) (Clark and Fritz, 1997; Campeau et al., 2017) in the riverbank sediments is less obvious.

Further along groundwater flowpaths 1 and 2, the δ^{13}C-DIC values increase from −9 ± 2‰ to +3 ± 2‰ with DIC becoming enriched in ^{13}C in the Holocene aquifer (Fig. 2 and Fig. 3B). In contrast, while progressing towards the RTZ and the Pleistocene aquifer, the decrease in δ^{13}C-DIC values to −17±2‰ indicates a preferential enrichment of ^{12}C-DIC in groundwater prior to a final increase to background values between −7 ± 2‰ and −13±2‰ in the Pleistocene wells most distant from the riverbank (Fig. 3B). These contrasting δ^{13}C-DIC isotopic shifts are likely caused by the succession of methanogenesis where CO_2 is consumed, followed by methanotrophy where CO_2 is produced, respectively (Murphy et al., 1989; Campeau et al., 2017).

3.5. Methane cycling

Along the groundwater flowpaths, CH_4 locally reaches very high concentrations of up to 58 mg/L, especially below the aquitard/aquifer hydraulic connections (Fig. 2). We suggest that the

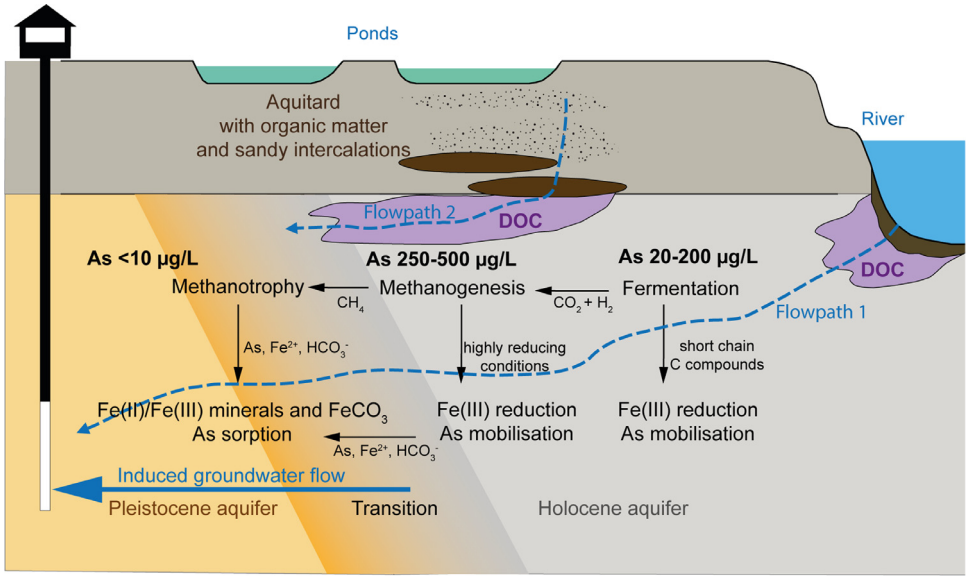

Fig. 4. Conceptual model of organic matter sources and cycling in As-contaminated aquifers. River water enriched with DOC infiltrates into the aquifer from riverbank sediments, promoting reducing processes such as fermentation and Fe(III) reduction. At the aquitard/aquifer hydraulic connections, additional DOC-enriched aquitard pore water infiltrates into the aquifer, thereby promoting methanogenesis. At the transition between the Holocene (grey) and the Pleistocene aquifers (orange), methanotrophy occurs while the intruding redox conditions dissolve Fe and As from the Pleistocene sands that consequently turn grey. However, net As immobilisation dominates, as a product of biotic and abiotic reactions involving Fe. An accelerated advection induced by large-scale groundwater extraction from Pleistocene aquifers can exacerbate the advection of reducing conditions and hence promote As mobilisation in previously low-As aquifers.

production of CH_4 in the Holocene aquifer is attributed to a two-step process involving (i) a substrate-producing fermentation step, and (ii) methanogenesis (Conrad et al., 2014; Glodowska et al., 2021). Furthermore, the decrease of methane concentrations across the RTZ and the enrichment in the DIC-isotopy is a strong indication of methanotrophy. The indicated methane cycling is corroborated by a recent microbial community analysis that showed the presence of both methanogenic and methanotrophic microorganisms in the Holocene aquifer and at the RTZ (i.e., *Methyloparacocci, Methylomonaceae, Candidatus Methanoperdens*) (Glodowska et al., 2020b, 2021).

The carbon isotope signatures of CH_4 (δ^{13}C-CH_4) span a remarkably wide range from −87±2‰ to +47±2‰ (Δ 134‰). In the Holocene aquifer, the low δ^{13}C-CH_4 signatures between −87±2‰ and −75±2‰ (Fig. 3C, grey dots) are typical for hydrogenotrophic methanogenesis, where the isotopically lighter $^{12}CO_2$ is kinetically favoured over $^{13}CO_2$ during transformation to CH_4 (Whiticar, 1999; Liu et al., 2009; Conrad et al., 2014; Campeau et al., 2017). Accordingly, the preferred consumption of $^{12}CO_2$ is reflected in the simultaneous increase of δ^{13}C in the bulk DIC (Fig. 3B and Fig. S3). Note that the isotopic shift of DIC is much lower than that of CH_4 because CO_2 has a high background concentration in the form of HCO_3^-.

The δ^{13}C-CH_4 signatures in three wells located within the Holocene aquifer along flowpath 2 (Fig. 4) are somewhat less negative (−76±2‰, wells 6a, 8a and 9a in Fig. 3C), while the CH_4 concentrations are 40–58 mg/L, which is close to or even above saturation at the given temperature and hydraulic pressure conditions (saturation approx. 43 to 63 mg/L for wells screened at 20 m and 30 m, respectively, considering an average water table level of 8 m b.g.l.). Therefore, and based on noble gas investigations in groundwater of these wells, we hypothesise that an interstitial free CH_4-gas phase has formed, which now occupies part of the pore space (Lightfoot et al., 2020), accompanied by a slight isotopic enrichment of CH_4 in groundwater, as the lighter $^{12}CH_4$ diffuses more easily into the gas phase than $^{13}CH_4$ (Xia and Tang, 2012).

Further along flowpath 2 into the RTZ and in the Pleistocene aquifer (Fig. 3C, yellow and brown dots), dissolved CH_4 decreases sharply to below 0.5 mg/L (wells 12 and 13a), while δ^{13}C-CH_4 values increase from −87±2‰ up to +47±2‰ (Δ+134‰). This is a strong indication of methane oxidation by methanotrophy, where the preferred consumption of the isotopically lighter $^{12}CH_4$ causes this remarkable isotopic enrichment. In turn, the CO_2 produced from methane oxidation is likely causing the observed decrease in δ^{13}C-DIC (Fig. 3B and Fig. S3). Finally, the resulting rise in HCO_3^- has most likely caused siderite ($FeCO_3$) oversaturation and precipitation, explaining the presence of the latter within the RTZ sediments (Kontny et al., 2021). This hypothesised precipitation of carbonates can also explain the lower δ^{13}C-DIC signatures observed within the RTZ as a result of the preferential precipitation of ^{13}C-carbonate.

4. Conclusions

As conceptually illustrated in Fig. 4, our hydrochemical and stable carbon isotope analyses suggest that fermentation, methanogenesis and methanotrophy can significantly affect carbon cycling in high-As aquifers. In previous analyses of As-contaminated sites, fermentative processes have largely been overlooked, even though these processes transform OM to small reactive molecules that can be utilized for methanogenesis and supply additional electron donating capacity for Fe(III) reduction. Therefore, fermentation likely has important implications for the mobilisation and subsequent fate of As.

Our study demonstrates that OM-rich pore waters infiltrating from aquitard sediments are accompanied by particularly high As concentrations in the aquifer, consistent with recent findings from other As-contaminated sites (Erban et al., 2013; Mihajlov et al., 2020). While slowly percolating through the aquitard, pore waters become enriched in DOC and NH_4^+ by the decomposition of sedimentary OM. During this percolation and/or upon egress into the aquifer, the DOC can locally promote methanogenesis and Fe(III) reduction, and thereby result in substantial As mobilisation in the affected parts of the aquifers (Fig. 4). Hence, such highly reducing, methanogenic zones likely contribute to the widely observed heterogeneity in groundwater As concentrations. At these locations,

oversaturation of methane can lead to the formation of interstitial gas bubbles (Lightfoot et al., 2020), which we hypothesize to locally obstruct the groundwater flow, as reported previously for petroleum contaminated aquifers (Amos et al., 2011), as well as for sites affected by denitrification and N_2 gas formation (Ryan et al., 2000). At our study site the overall effect of slow transport processes, and accordingly sufficiently long reaction times for the development of highly reducing conditions, is reflected in particularly high As concentrations >200 µg/L (i.e., >20 times the WHO guideline value) that are predominantly found under methanogenic conditions.

Furthermore, our new data provide for the first time field-based hydrochemical and isotopic evidence for methanotrophy to occur where CH_4-enriched groundwater infiltrating from the Holocene aquifer comes in contact with the abundant Fe(III) (oxyhydr)oxides contained in the Pleistocene sediments (Fig. 4, flowpath 2). This field observation is consistent with recent results of laboratory incubation experiments with Pleistocene sediments from the RTZ at our field site, which demonstrated the occurrence of CH_4 oxidation coupled with Fe(III) reduction and As mobilisation (Glodowska et al., 2020b). Interestingly, this finding is also in line with investigations carried out at a crude oil-contaminated site in Minnesota (USA), where methanogenesis coupled to iron reduction in the anaerobic core of the plume was shown to be an important process (Amos et al., 2011, 2012). Consequently, the As retardation capacity, previously attributed to the high sorption capacity of RTZ sediments, specifically that associated with Fe(II/III) and Fe(III)-minerals (Eiche et al., 2008; Rathi et al., 2017; Neidhardt et al., 2018; Kontny et al., 2021), might be reduced under methanotrophic conditions.

Here we showed how methane cycling contributes to the patchiness of redox conditions in aquifers and hence to the variability in groundwater of As concentrations, particularly in aquifer zones characterized by slow advection (flowpath 2, Fig. 4). In contrast, in the more permeable aquifer sections where higher flow velocities persist (flowpath 1, Fig. 4), methane cycling plays a minor role and As concentrations remain lower. Nevertheless, overall mass fluxes of As will be largely controlled by these more permeable zones. Eventually, both regimes (high As conc./small flux vs lower As conc./high flux) need to be understood and considered in any risk assessment as well as in the development of groundwater management and remediation strategies.

Declaration of Competing Interest

The authors declare that they have no known competing financial interests or personal relationships that could have appeared to influence the work reported in this paper.

Acknowledgements

We thank the Swiss National Science Foundation SNSF (grant 200021E-167821) and the Deutsche Forschungsgemeinschaft DFG (grants KA 1736/41–1 and NE687/8–1) for funding the AdvectAs project. We are grateful to C. Stengel for stable water isotopes analyses and for her technical assistance along with N. Pfenninger for the ICP-MS analyses. Thanks are also extended to the AuA laboratory, Eawag, for their support with the hydrochemical analyses. Our gratitude goes to S. Robert and P. Kathriner, SURF Department Eawag, for their support with methane sampling and methane isotopic analyses. We thank T. R. Maddox and his Stable Isotope Ecology Laboratory, University of Georgia, for the isotopic analyses of DIC, DOC and NH_4^+. Our gratitude also goes to M. Brennwald and R. Britt, Eawag, and to Anh Lang T. and Thanh Nguyen V., KLATEFOS, for assistance during the field campaigns. We are also grateful to the whole community of Van Phuc for their kind collaboration.

Supplementary materials

Supplementary material associated with this article can be found, in the online version, at doi:10.1016/j.watres.2021.117300.

References

Amos, R.T., Bekins, B.A., Cozzarelli, I.M., Voytek, M.A., Kirshtein, J.D., Jones, E.J.P., Blowes, D.W., 2012. Evidence for iron-mediated anaerobic methane oxidation in a crude oil-contaminated aquifer. Geobiology 10, 506–517.
Amos, R.T., Bekins, B.A., Delin, G.N., Cozzarelli, I.M., Blowes, D.W., Kirshtein, J.D., 2011. Methane oxidation in a crude oil contaminated aquifer: delineation of aerobic reactions at the plume fringes. J. Contam. Hydrol. 125, 13–25.
Berg, M., Stengel, C., Trang, P.T.K., Viet, P.H., Sampson, M.L., Leng, M., Samreth, S., Fredericks, D., 2007. Magnitude of arsenic pollution in the Mekong and Red River Deltas — Cambodia and Vietnam. Science of The Total Environ. 372, 413–425.
Berg, M., Trang, P.T.K., Stengel, C., Buschmann, J., Viet, P.H., Dan, N.V., Giger, W., Stüben, D., 2008. Hydrological and sedimentary controls leading to arsenic contamination of groundwater in the Hanoi area, Vietnam: the impact of iron-arsenic ratios, peat, river bank deposits, and excessive groundwater abstraction. Chem. Geol. 249, 91–112.
Bostick, B.C., Fendorf, S., 2003. Arsenite sorption on troilite (FeS) and pyrite (FeS2). Geochim. Cosmochim. Acta 67, 909–921.
Botsch, K.C., Conrad, R., 2011. Fractionation of stable carbon isotopes during anaerobic production and degradation of propionate in defined microbial cultures. Org. Geochem. 42, 289–295.
Buschmann, J., Berg, M., 2009. Impact of sulfate reduction on the scale of arsenic contamination in groundwater of the Mekong, Bengal and Red River deltas. Applied Geochemistry 24, 1278–1286.
Campeau, A., Wallin, M.B., Giesler, R., Löfgren, S., Mörth, C.-.M., Schiff, S., Venkiteswaran, J.J., Bishop, K., 2017. Multiple sources and sinks of dissolved inorganic carbon across Swedish streams, refocusing the lens of stable C isotopes. Sci Rep 7, 9158.
Chapelle, F.H., 2000. Ground-Water Microbiology and Geochemistry. John Wiley & Sons, New York.
Clark, I.D., Fritz, P., 1997. Environmental Isotopes in Hydrogeology. Lewis Publishers, New York.
Conrad, R., Claus, P., Chidthaisong, A., Lu, Y., Fernandez Scavino, A., Liu, Y., Angel, R., Galand, P.E., Casper, P., Guerin, F., Enrich-Prast, A., 2014. Stable carbon isotope biogeochemistry of propionate and acetate in methanogenic soils and lake sediments. Org. Geochem. 73, 1–7.
Cozzarelli, I.M., Schreiber, M.E., Erickson, M.L., Ziegler, B.A., 2016. Arsenic Cycling in Hydrocarbon Plumes: secondary Effects of Natural Attenuation. Groundwater 54, 35–45.
Eiche, E., Berg, M., Hönig, S.-.M., Neumann, T., Lan, V.M., Pham, T.K.T., Pham, H.V., 2017. Origin and availability of organic matter leading to arsenic mobilisation in aquifers of the Red River Delta, Vietnam. Appl. Geochem. 77, 184–193.
Eiche, E., Neumann, T., Berg, M., Weinman, B., van Geen, A., Norra, S., Berner, Z., Trang, P.T.K., Viet, P.H., Stüben, D., 2008. Geochemical processes underlying a sharp contrast in groundwater arsenic concentrations in a village on the Red River delta, Vietnam. Appl. Geochem. 23, 3143–3154.
Erban, L.E., Gorelick, S.M., Zebker, H.A., Fendorf, S., 2013. Release of arsenic to deep groundwater in the Mekong Delta, Vietnam, linked to pumping-induced land subsidence. Proceed. Nat. Acad. Sci. 110, 13751.
Fendorf, S., Michael, H.A., van Geen, A., 2010. Spatial and Temporal Variations of Groundwater Arsenic in South and Southeast Asia. Science 328, 1123.
Fry, B., Sherr, E.B., 1984. DELTA-C-13 MEASUREMENTS AS INDICATORS OF CARBON FLOW IN MARINE AND FRESH-WATER ECOSYSTEMS. Contrib. Mar. Sci. 27, 13–47.
Glodowska, M., Stopelli, E., Schneider, M., Lightfoot, A., Rathi, B., Straub, D., Patzner, M., Duyen, V.T., Berg, M., Kleindienst, S., Kappler, A., 2020a. Role of in Situ Natural Organic Matter in Mobilizing As during Microbial Reduction of Fel-II-Mineral-Bearing Aquifer Sediments from Hanoi (Vietnam). Environ. Sci. Technol. 54, 4149–4159.
Glodowska, M., Stopelli, E., Schneider, M., Rathi, B., Straub, D., Lightfoot, A., Kipfer, R., Berg, M., Jetten, M., Kleindienst, S., Kappler, A., 2020b. Arsenic mobilization by anaerobic iron-dependent methane oxidation. Commun. Earth Environ. 1, 42.
Glodowska, M., Stopelli, E., Straub, D., Vu Thi, D., Trang, P.T.K., Viet, P.H., AdvectAs Team, Berg, M., Kappler, A., Kleindienst, S., 2021. Arsenic behavior in groundwater in Hanoi (Vietnam) influenced by a complex biogeochemical network of iron, methane, and sulfur cycling. J. Hazard. Mater. 407, 124398.
Hammer, Ø., Harper, D.A.T., Ryan, P.D., 2001. PAST: paleontological statistics software package for education and data analysis. Palaeontologia Electronica 4, 1–9.
Harvey, C.F., Swartz, C.H., Badruzzaman, A.B.M., Keon-Blute, N., Yu, W., Ali, M.A., Jay, J., Beckie, R., Niedan, V., Brabander, D., Oates, P.M., Ashfaque, K.N., Islam, S., Hemond, H.F., Ahmed, M.F., 2002. Arsenic Mobility and Groundwater Extraction in Bangladesh. Science 298, 1602.
Holmes, R.M., McClelland, J.W., Sigman, D.M., Fry, B., Peterson, B.J., 1998. Measuring 15N–NH4+ in marine, estuarine and fresh waters: an adaptation of the ammonia diffusion method for samples with low ammonium concentrations. Mar Chem 60, 235–243.
Islam, F.S., Gault, A.G., Boothman, C., Polya, D.A., Charnock, J.M., Chatterjee, D., Lloyd, J.R., 2004. Role of metal-reducing bacteria in arsenic release from Bengal delta sediments. Nature 430, 68–71.

Karagas, M.R., Gossai, A., Pierce, B., Ahsan, H., 2015. Drinking Water Arsenic Contamination, Skin Lesions, and Malignancies: a Systematic Review of the Global Evidence. Curr Environ Health Rep 2, 52–68.
Kontny, A., Schneider, M., Eiche, E., Stopelli, E., Glodowska, M., Rathi, B., Göttlicher, J., Byrne, J.M., Kappler, A., Berg, M., Duyen, T.V., Trang, P.T.K., Viet, P.H., Neumann, T., 2021. Iron mineral transformations and their impact on As (im)mobilization at redox interfaces in As-contaminated aquifers. Geochim. Cosmochim. Acta 296, 189–209.
Kulkarni, H.V., Mladenov, N., Johannesson, K.H., Datta, S., 2017. Contrasting dissolved organic matter quality in groundwater in Holocene and Pleistocene aquifers and implications for influencing arsenic mobility. Appl. Geochem. 77, 194–205.
Lawson, M., Polya, D.A., Boyce, A.J., Bryant, C., Ballentine, C.J., 2016. Tracing organic matter composition and distribution and its role on arsenic release in shallow Cambodian groundwaters. Geochim. Cosmochim. Acta 178, 160–177.
Lightfoot, A., Brennwald, M., Kipfer, R., 2020. The Role of Gases in an Arsenic Contaminated Aquifer. EGU General Assembly 2020, 10245. doi:10.5194/egusphere-egu2020-10245.
Liu, T.-K., Chen, K.-Y., Yang, T.F., Chen, Y.-G., Chen, W.-F., Kang, S.-C., Lee, C.-P., 2009. Origin of methane in high-arsenic groundwater of Taiwan – Evidence from stable isotope analyses and radiocarbon dating. J. Asian Earth Sci. 36, 364–370.
McArthur, J.M., Banerjee, D.M., Hudson-Edwards, K.A., Mishra, R., Purohit, R., Ravenscroft, P., Cronin, A., Howarth, R.J., Chatterjee, A., Talukder, T., Lowry, D., Houghton, S., Chadha, D.K., 2004. Natural organic matter in sedimentary basins and its relation to arsenic in anoxic ground water: the example of West Bengal and its worldwide implications. Appl. Geochem. 19, 1255–1293.
McMahon, P.B., Chapelle, F.H., 1991. Microbial production of organic acids in aquitard sediments and its role in aquifer geochemistry. Nature 349, 233–235.
Mihajlov, I., Mozumder, M.R.H., Bostick, B.C., Stute, M., Mailloux, B.J., Knappett, P.S.K., Choudhury, I., Ahmed, K.M., Schlosser, P., van Geen, A., 2020. Arsenic contamination of Bangladesh aquifers exacerbated by clay layers. Nat Commun 11, 2244.
Murphy, E.M., Davis, S.N., Long, A., Donahue, D., Jull, A.J.T., 1989. Characterization and isotopic composition of organic and inorganic carbon in the Milk River Aquifer. Water Resour Res. 25, 1893–1905.
Neidhardt, H., Winkel, L.H.E., Kaegi, R., Stengel, C., Trang, P.T.K., Lan, V.M., Viet, P.H., Berg, M., 2018. Insights into arsenic retention dynamics of Pleistocene aquifer sediments by in situ sorption experiments. Water Res. 129, 123–132.
Neumann, R.B., Ashfaque, K.N., Badruzzaman, A.B.M., Ashraf Ali, M., Shoemaker, J.K., Harvey, C.F., 2010. Anthropogenic influences on groundwater arsenic concentrations in Bangladesh. Nat Geosci. 3, 46–52.
Nghiem, A.A., Shen, Y., Stahl, M., Sun, J., Haque, E., DeYoung, B., Nguyen, K.N., Thi Mai, T., Trang, P.T.K., Viet, P.H., Mailloux, B., Harvey, C.F., van Geen, A., Bostick, B.C., 2020. Aquifer-Scale Observations of Iron Redox Transformations in Arsenic-Impacted Environments to Predict Future Contamination. Environ. Sci. Technol. Lett. 7, 916–922.
Parkhurst, D.L., Appelo, C.A.J., 2013. Description of input and examples for PHREEQC version 3: a computer program for speciation, batch-reaction, one-dimensional transport, and inverse geochemical calculations. U.S. Geological Survey Techniques and Methods 497. book 6, chap. A43 https://pubs.usgs.gov/tm/06/a43/ .
Podgorski, J., Berg, M., 2020. Global threat of arsenic in groundwater. Science 368, 845–850.
Polizzotto, M.L., Kocar, B.D., Benner, S.G., Sampson, M., Fendorf, S., 2008. Near-surface wetland sediments as a source of arsenic release to ground water in Asia. Nature 454, 505–508.
Polya, D.A., Sparrenbom, C., Datta, S., Guo, H., 2019. Groundwater arsenic biogeochemistry – Key questions and use of tracers to understand arsenic-prone groundwater systems. Geoscience Frontiers 10, 1635–1641.
Postma, D., Larsen, F., Thai, N.T., Trang, P.T.K., Jakobsen, R., Nhan, P.Q., Long, T.V., Viet, P.H., Murray, A.S., 2012. Groundwater arsenic concentrations in Vietnam controlled by sediment age. Nat. Geosci. 5, 656–661.
Postma, D., Pham, T.K.T., Sø, H.U., Hoang, V.H., Vi, M.L., Nguyen, T.T., Larsen, F., Pham, H.V., Jakobsen, R., 2016. A model for the evolution in water chemistry of an arsenic contaminated aquifer over the last 6000years, Red River floodplain, Vietnam. Geochim. Cosmochim. Acta 195, 277–292.
Rathi, B., Neidhardt, H., Berg, M., Siade, A., Prommer, H., 2017. Processes governing arsenic retardation on Pleistocene sediments: adsorption experiments and model-based analysis. Water Resour. Res. 53, 4344–4360.
Richards, L.A., Magnone, D., Sültenfuß, J., Chambers, L., Bryant, C., Boyce, A.J., van Dongen, B.E., Ballentine, C.J., Sovann, C., Uhlemann, S., Kuras, O., Gooddy, D.C., Polya, D.A., 2019. Dual in-aquifer and near surface processes drive arsenic mobilization in Cambodian groundwaters. Sci. Environ. 659, 699–714.
Rowland, H.A.L., Pederick, R.L., Polya, D.A., Pancost, R.D., Van Dongen, B.E., Gault, A.G., Vaughan, D.J., Bryant, C., Anderson, B., Lloyd, J.R., 2007. The control of organic matter on microbially mediated iron reduction and arsenic release in shallow alluvial aquifers. Cambodia. Geobiol. 5, 281–292.
Ryan, M.C., MacQuarrie, K.T.B., Harman, J., McLellan, J., 2000. Field and modeling evidence for a "stagnant flow" zone in the upper meter of sandy phreatic aquifers. J. Hydrol. (Amst) 233, 223–240.
Smedley, P.L., Kinniburgh, D.G., 2002. A review of the source, behaviour and distribution of arsenic in natural waters. Appl. Geochem. 17, 517–568.
Smith, A.H., Lingas, E.O., Rahman, M., 2000. Contamination of drinking-water by arsenic in Bangladesh: a public health emergency. Bull. World Health Org. 78, 1093–1103.
Sø, H.U., Postma, D., Vi, M.L., Pham, T.K.T., Kazmierczak, J., Dao, V.N., Pi, K., Koch, C.B., Pham, H.V., Jakobsen, R., 2018. Arsenic in Holocene aquifers of the Red River floodplain, Vietnam: effects of sediment-water interactions, sediment burial age and groundwater residence time. Geochim. Cosmochim. Acta 225, 192–209.
Sracek, O., Berg, M., Müller, B., 2018. Redox buffering and de-coupling of arsenic and iron in reducing aquifers across the Red River Delta, Vietnam, and conceptual model of de-coupling processes. Environ. Sci. Pollut. Res. 25, 15954–15961.
Stahl, M.O., Harvey, C.F., van Geen, A., Sun, J., Thi Kim Trang, P., Mai Lan, V., Mai Phuong, T., Hung Viet, P., Bostick, B.C., 2016. River bank geomorphology controls groundwater arsenic concentrations in aquifers adjacent to the Red River, Hanoi Vietnam. Water Resour. Res. 52, 6321–6334.
Stopelli, E., Duyen, V.T., Mai, T.T., Trang, P.T.K., Viet, P.H., Lightfoot, A., Kipfer, R., Schneider, M., Eiche, E., Kontny, A., Neumann, T., Glodowska, M., Patzner, M., Kappler, A., Kleindienst, S., Rathi, B., Cirpka, O., Bostick, B., Prommer, H., Winkel, L.H.E., Berg, M., 2020. Spatial and temporal evolution of groundwater arsenic contamination in the Red River delta, Vietnam: interplay of mobilisation and retardation processes. Sci. Total Environ. 717, 137143.
Stuckey, Jason W., Schaefer, Michael V., Kocar, Benjamin D., Benner, Shawn G., Fendorf, S., 2016. Arsenic release metabolically limited to permanently water-saturated soil in Mekong Delta. Nat. Geosci. 9, 70–76.
Trung, D.T., Nhan, N.T., Don, T.V., Hung, N.K., Kazmierczak, J., Nhan, P.Q., 2020. The controlling of paleo-riverbed migration on Arsenic mobilization in groundwater in the Red River Delta, Vietnam. VIETNAM J. EARTH SCI. 42 (2), 2020.
van Geen, A., Bostick, B.C., Trang, P.T.K., Lan, V.M., Mai, N.-N., Manh, P.D., Viet, P.H., Radloff, K., Aziz, Z., Mey, J.L., Stahl, M.O., Harvey, C.F., Oates, P., Weinman, B., Stengel, C., Frei, F., Kipfer, R., Berg, M., 2013. Retardation of arsenic transport through a Pleistocene aquifer. Nature 501, 204–207.
van Geen, A., Zheng, Y., Cheng, Z., Aziz, Z., Horneman, A., Dhar, R.K., Mailloux, B., Stute, M., Weinman, B., Goodbred, S., Seddique, A.A., Hoque, M.A., Ahmed, K.M., 2006. A transect of groundwater and sediment properties in Araihazar, Bangladesh: further evidence of decoupling between As and Fe mobilization. Chem. Geol. 228, 85–96.
Wallis, I., Prommer, H., Berg, M., Siade, A.J., Sun, J., Kipfer, R., 2020. The river–groundwater interface as a hotspot for arsenic release. Nat. Geosci. 13, 288–295.
Whiticar, M.J., 1999. Carbon and hydrogen isotope systematics of bacterial formation and oxidation of methane. Chem. Geol. 161, 291–314.
WHO, 2011. Guidelines For Drinking-water Quality, 4th edition.
Xia, X., Tang, Y., 2012. Isotope fractionation of methane during natural gas flow with coupled diffusion and adsorption/desorption. Geochim. Cosmochim. Acta 77, 489–503.
Zhang, J., Ma, T., Feng, L., Yan, Y., Abass, O.K., Wang, Z., Cai, H., 2017. Arsenic behavior in different biogeochemical zonations approximately along the groundwater flow path in Datong Basin, northern China. Sci. Total Environ. 584-585, 458–468.
Ziegler, B.A., Schreiber, M.E., Cozzarelli, I.M., Crystal Ng, G.H., 2017. A mass balance approach to investigate arsenic cycling in a petroleum plume. Environ. Pollut. 231, 1351–1361.